



3D inverse modeling of electrical resistivity and induced polarization data versus geostatistical-based modeling

Mahmoud Babaei, Maysam Abedi *, Gholam Hossain Norouzi, Saeed Kazem Alilou

School of Mining Engineering, College of Engineering, University of Tehran, Tehran, Iran

Received: 29 July 2020, Revised: 26 January 2021, Accepted: 21 February 2021
© University of Tehran

Abstract

This work aims to compare the 3D geophysical inversion models of electrical resistivity and chargeability with the 3D geostatistical-based models interpolated from 2D inversion of electrical data. The Takht-e-Gonbad Cu deposit situated in the central domain of Iran is chosen to find out the spatial correlation of the porphyry-type ore deposition with the electrical properties. Assuming an ordinary kriging algorithm, the inverted 2D electrical models were interpolated in 3D domain to provide insights about the geometry of Cu-bearing mineralization. Higher values of electrical resistivity and chargeability corresponded to the anomalous zones of Cu mineralization through a fractal analysis of concentration-number (C-N) model derived from exploratory drillings. Surveyed geophysical data were also inverted directly in 3D electrical models to compare them with the geostatistical models, showing that the 3D inversion could much better preserve the geometry of the Cu occurrences, and their classified fractal models were much in close association to each other. The correlation coefficients between the 3D electrical models and the Cu concentration were higher than the geostatistical models, and there is clearly information in the inversion result that is not being captured in the geostatistical interpolation. The significance of this study lies in improvement of the performance of 3D inversion methodology over 3D geostatistical interpolation.

Keywords: Electrical Resistivity, Electrical Chargeability, Geostatistics, Inversion, Takht-e-Gonbad Deposit

Introduction

The NW Kerman province of Iran is one of the richest mineralization area for porphyry-type Cu occurrences, in which the Sirjan mineralization district has been widely investigated through analyzing exploratory data in several retrospective studies (e.g. Izadi Yazdanabadi et al., 2017; Afzal et al., 2016). Among enormous Cu deposits in this region, the Takht-e-Gonbad Cu deposit is chosen as a case study in this work to construct the geometry of Cu resource through an integrated analysis of geophysical data, while the performance of inverse modeling and geostatistical interpolation is profoundly examined. To construct a reliable geometry of an ore deposit, geophysical models are inevitable to delineate the location of anomalous zones and exploratory drillings (Aguilef et al., 2017).

Integrated geophysical methods are prevalent in mineral exploration to attain qualified results with lower uncertainty in delineation of a sought target by reducing the ambiguities arising from single geophysical data (Mostafaie & Ramazi, 2015). From a geophysical standpoint, the ultimate goal of all geophysical surveys is the detection of physical property contrasts of

* Corresponding author e-mail: maysamabedi@ut.ac.ir

materials (Telford et al., 1990). To get more reliable results in exploration of porphyry-type targets, different geophysical techniques such as induced polarization (IP) and direct current electrical resistivity (Res) have been widely used because of its low operational costs and environmental damages (Sultan et al., 2009). Inverse modeling and interpretation of a varieties of porphyry-type targets have attracted attention of scholars (e.g. Oldenburg et al., 1997; Saein et al., 2012). In addition to geophysical data inversion, there are numerous methods that deal with interpolation of sparse data set based on the nature of the desired data. When there are lack of electrical data or 3D inversion is time consuming and is actually rather difficult to implement in practice, 2D inversion is superior to 3D modeling by imaging physical properties from Res and IP data. Note that these 2D physical properties can in turn be interpolated in 3D straight away to better present the geometry of sought target.

Interpolation approaches are categorized into two main groups that are statistical (classical) and geostatistical ones. On the geostatistical theory, spatial correlation of the desired variable(s) affects the interpolation result by imposing the range, anisotropy and continuity of the data in the algorithm (Aguilef et al., 2017), leading to great improvement in identifying the locations, general geometry, and boundaries of the true variable(s).

Several researches have been pertained to simultaneously consider geophysical and geostatistical data modeling. Among lots of studies, Babaei et al., 2019 has geostatistically interpolated 2D inverted electrical models into 3D, where the geometry of sought ore-bearing target was in close association to the electrical resistivity and chargeability models. Abedi et al., 2015 have utilized a magnetic susceptibility property as a secondary soft and dense variable by inverting magnetometry data to estimate the grade of Fe (primary variable) for a deposit target, where a sparse pattern of exploratory drilling was available. Those variables had a meaningful spatial correlation as well. In electrical geophysics following the same line of thought as Abedi et al., 2015, Asghari et al., 2016 examined multivariate geostatistics on geo-electrical properties to estimate Cu grade with lower amounts of estimation variance and model uncertainty. They generated a sulfide factor variable (as a ratio of the electrical chargeability to the electrical resistivity) by inverse modeling of the electrical data to provide a correlated secondary variable for Cu grade estimation. For aforementioned real cases, outputs verified that incorporating a soft variable drastically outperforms the results over the cases of single variable estimates (Babaei et al., 2019).

This work aims to compare the 3D geophysical models of electrical resistivity and chargeability derived from 3D inversion, and 3D geostatistical-based interpolation. For 3D interpolation, geophysical models were inverted in 2D space in our previous study (Babaei et al., 2019), then geo-electrical properties were interpolated in 3D through a kriging algorithm. Here, we want to investigate the efficiency of such statistical models with the geophysical models when implementing a 3D inversion algorithm. On the basis of exploratory drilling, the spatial correlations of geophysical models are calculated against the Cu concentration for a revisited real case study in the Takht-e-Gonbad Porphyry Cu Deposit, Kerman province of Iran. In addition, all models are classified into some populations through a fractal analysis to determine the efficiency of 3D inverse modeling and geostatistical interpolation for recovering the geometry of a sought Cu-bearing target.

This work has been presented in the fifth sections. The second section describes the geological descriptions of the Takht-e-Gonbad Porphyry-Cu deposit and all exploratory drillings. In the third section, the configuration of geo-electrical surveys is explained; then a 2D inverse modeling algorithm is implemented for a more complete set of electrical data (compared to our previous electrical data set in Babaei et al., 2019) to construct physical models of electrical resistivity and chargeability. These models are interpolated in 3D through an ordinary kriging. The 3D inversion of geophysical data is run to compare the acquired physical properties with the interpolated ones. A concentration-number (C-N) fractal curve of each geophysical

model is also plotted to discretize the model domain into some populations, where the most favorable one in association with the Cu ore occurrences are searched. In the section four as a discussion, the spatial correlation of interpolated and inverted models against the Cu concentration are discussed to evaluate the efficiency of each methodology in localizing the main body of the sought Cu-bearing target. Finally, all achievements are summarized in the conclusion section.

Geological descriptions of the studied area

The Takht-e-Gonbad porphyry Cu-bearing deposit is situated in the central domain geological setting of Iran, 80 km away at the NE of Sirjan, Kerman province. This active mine is intimately linked to a wide favorable mineralization belt named the Urmia-Dokhtar magmatic assemblage (UDMA) portrayed in Fig.1 (Aguilef et al., 2017), where volcanic-pyroclastic units of Eocene age with a dominant NE-SW trends have covered the area (Fig. 2a). Upon Yugoslavian geologists' reports, volcanic tuffs are hosted the Cu mineralization (Saric & Mijalkovic, 1973). It's worth pointing out that such mineralization and relevant alteration zones are associated with Miocene granodiorite rocks, intruded the Eocene volcanic-pyroclastic units.

Porphyry-Cu mineralization has occurred in the shape of veins, veinlets and disseminations, embedded in thermally metamorphosed and skarnized pyroclastic rocks, and in porphyritic intrusions (Hosseini et al., 2017; Mohammadi & Hezarkhani, 2018). Phyllic, propylitic, silicic and carbonate are the foremost alterations sporadically distributed in the study area. Note that phyllic alteration is more widespread and intensive over the tuffs and micro-granodiorite intrusions.

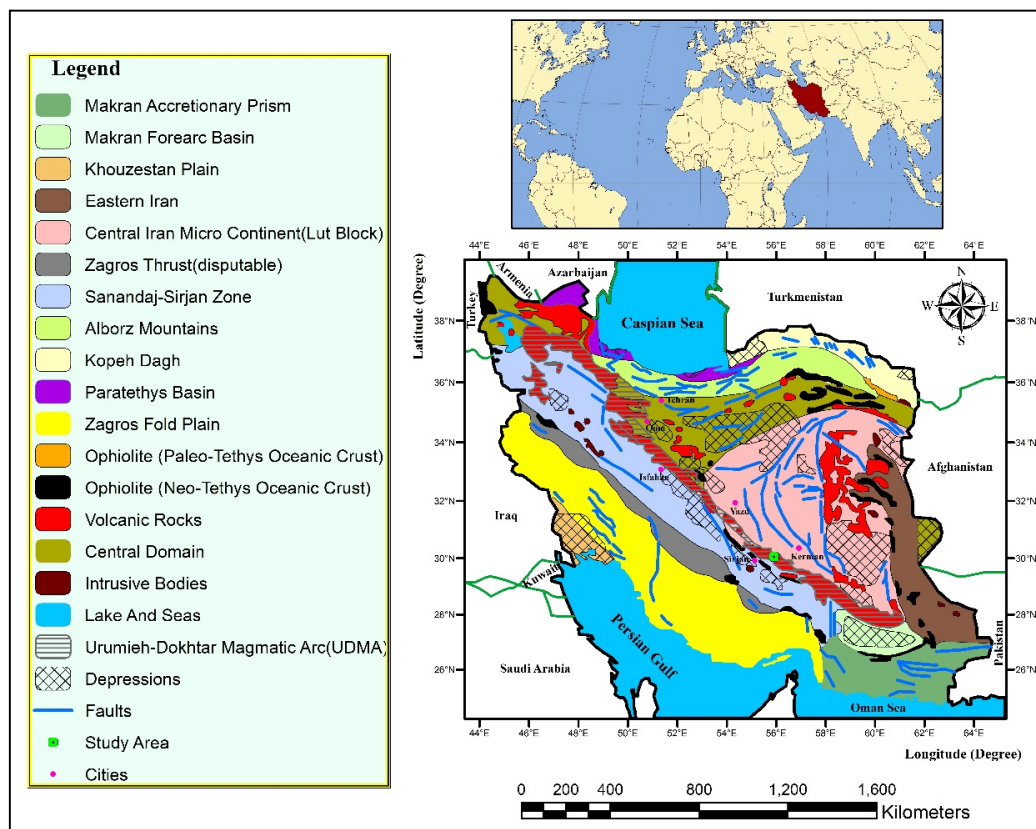


Figure 1. Structural Geology map of Iran, where the location of the studied region was presented at the central portion, over the Central Iran Block zone (reproduced from open access maps by the Geological Survey of Iran, GSI)

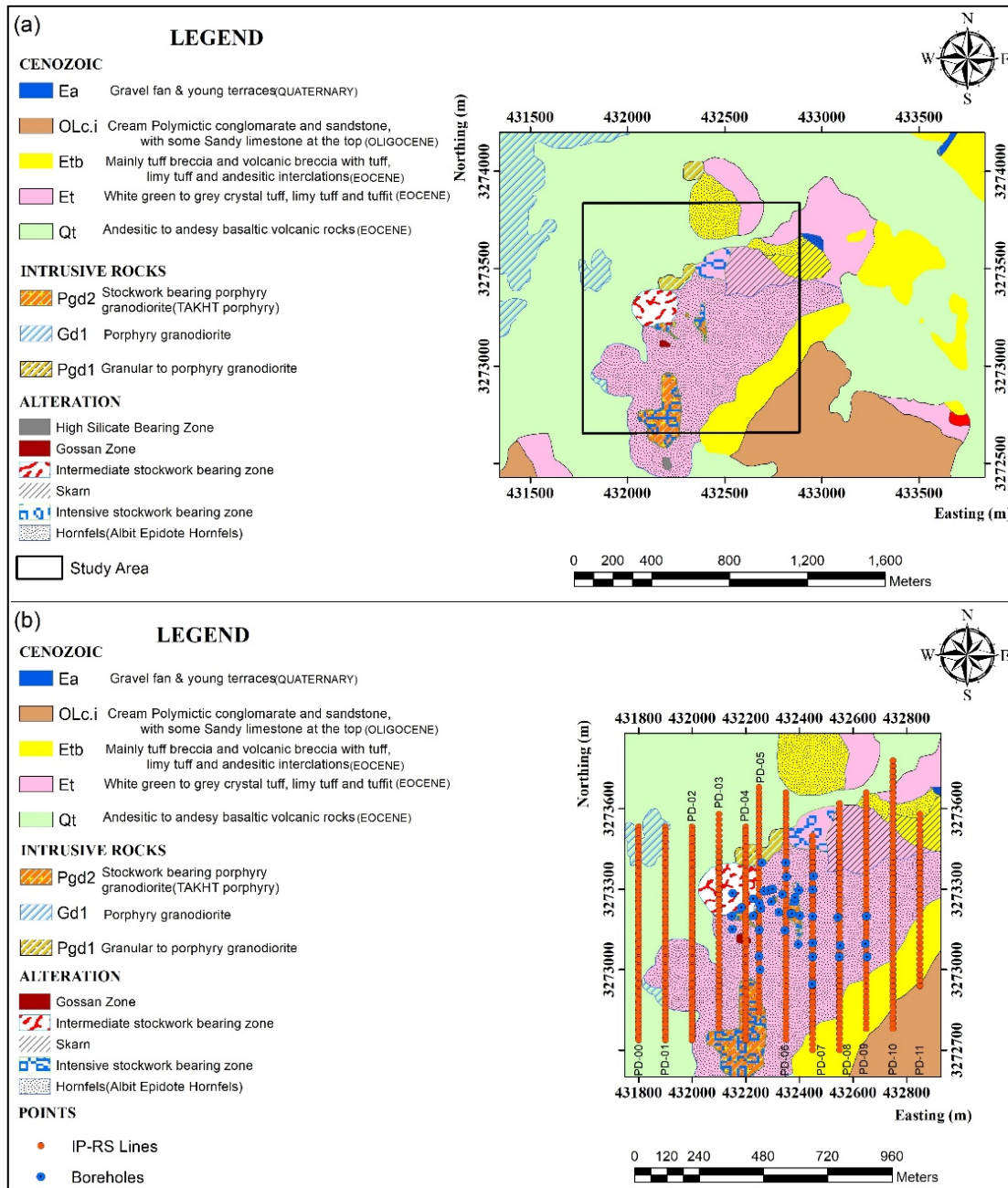


Figure 2. Location and geology map of the Takht-e-Gonbad porphyry Cu deposit (a), on which 2D electrical tomography profiles and drilled boreholes have been superimposed (b) (reproduced from open access maps by the Geological Survey of Iran, GSI)

Besides, this alteration is closely associated with Cu-bearing mineralization in the hypogene zone with trace minerals such as sericite (muscovite, illite), quartz, and subordinate chlorite, pyrite and chalcopyrite. Argillic or intermediate argillic alteration is the most extensive and common type of alteration for many porphyry-type Cu-bearing mineralization systems (e.g. Ranjbar et al., 2004; Alirezaei & Hassanpour, 2011; Fakhari et al., 2019). This alteration generates from the alteration of plagioclase with traces as kaolinite, illite, smectite, and montmorillonite. The argillic alteration is widespread at surface exposures and at shallow depths. Propylitic alteration occurs along irregular zones around the center of deposit, which are traced by minerals of chlorite, calcite, epidote and lower amounts of zeolite and amphibole

(Hosseini et al., 2017; Mohammadi & Hezarkhani, 2018).

Chalcopyrite is the main ore mineral in the hypogene zone, where pyrite and minor magnetite along veins are available, often found over the granodiorite and tuff units. The economic Cu grade of the hypogene zone has occurred about 150 m below the oxide cap (Hosseini, 2012; Afzal et al., 2016). Note that in the oxide zone, chalcopyrite was converted to the copper carbonate such as malachite. In the Takht-e-Gonbad deposit, mineralized portions have been developed in a transitional zone of hypogene, immature supergene and oxide zones. The thickness of enriched supergene zone is 10-50 m, characterized mainly by chalcocite and covellite (Hosseini, 2012; Hosseini et al., 2017). The study area locates within an active tectonic setting with dextral strike-slip lineaments, cut by the Nain-Baft and Chahar Gonbad faults in the south portions. Surface geological evidences indicate that Cu has been deposited mostly with an E-W strike (Mohammadi & Hezarkhani, 2018; Hosseini et al., 2011).

Geo-electrical survey

Geophysical survey was employed to investigate the electrical resistivity and chargeability models of the Cu-bearing targets in the Takht-e-Gonbad porphyry deposit. In concordance with the dispersion nature of Cu mineralization observed in outcropped rocks, twelve direct current 2D geo-electrical profiles were deployed perpendicular to the probable strike of ore-trapping system along a N-S direction. Figure 2b shows an enlarged view map of the geological setting of the prospect zone, on which the layout of the 2D electrical profiles and drillings were superimposed. The pole-dipole electrical array was run to measure data according to the depth of mineralization and surveying conditions. Such electrical configuration has higher depth of investigation, leading to more efficient field operation and also a high rate of data collection. The smoothness-constrained least-squares approach (deGroot-Hedlin & Constable, 1990; Sasaki, 1992; Loke et al., 2003) was run to invert all 2D electrical profiles, where it attempts to minimize the square of difference between the measured and calculate apparent resistivity values, and works well in cases that data have been corrupted by random or Gaussian noise.

Twelve electrical profiles were survey from west to east of the studied area shown in Fig.2b, which are named as PD-00, PD-01, PD-02, PD-03, PD-04, PD-05, PD-06, PD-07, PD-08, PD-09, PD-10 and PD-11, respectively. PD-04 to PD-07 were surveyed on the main source of Cu deposition. Along all 2D electrical profiles high quality data were measured with a spacing of 100 m, except PD-04 to PD-05 that is 50m. The electrode spacing of the PD-00, PD-01, PD-02, and PD04 is about 30 m, the rest is 40 m. Profiles PD-00 to PD-03 from the west and PD-10 and PD-11 from the east of the ore body are not crossing the boreholes, but other ones less and more cover the boreholes. Some new profiles with higher quality data measurements were inserted in comparison to the previous work by Babaei et al. (2020) to better construct geophysical models of the sought deposit. Figure 3 presents the 3D visualization of all forty drilled holes, on which a topography surface has been superimposed. The statistical descriptions of all drillings and core analysis of Cu grade have been tabulated in the last row of Table 1.

Table 1. Statistical summary of the drilled boreholes and electrical models

Data set	Mean	Variance	Max	Median	Min
Res-2D (Ωm)	137.16	23792.75	999.9	86.92	1.66
IP-2D (ms)	21.786	211.786	100.00	18.78	0.50
Res-3D (Ωm)	114.09	8808.85	985.29	83.73	8.03
IP-3D (ms)	21.819	175.423	71.29	18.59	1.13
Cu (%)	0.39624	0.14845	2.5700	0.3072	0.0014

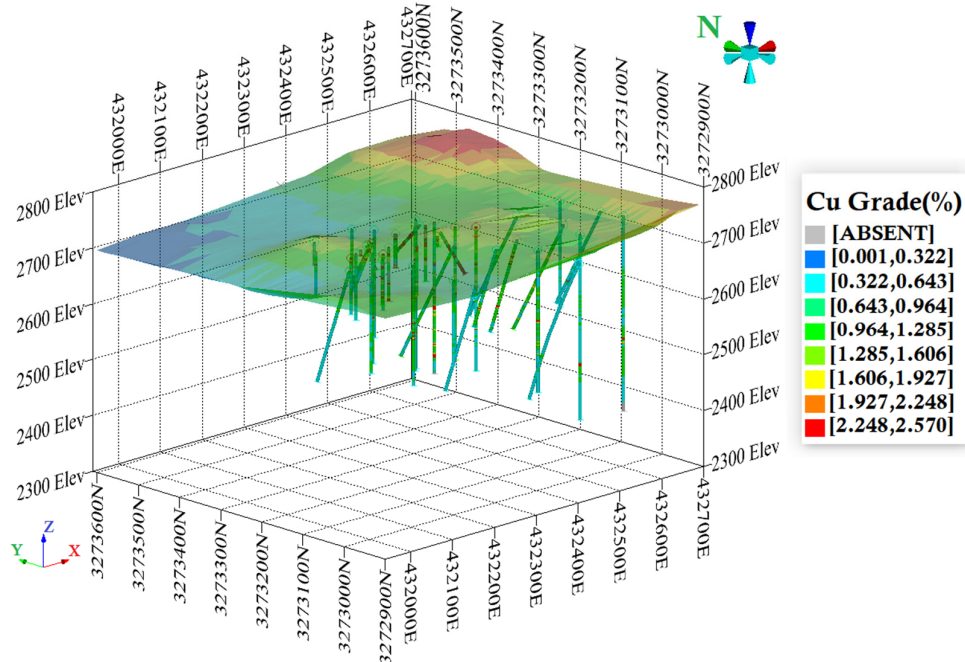


Figure 3. Location map of boreholes with topography surface in the studied region, where the sulfide-content Cu grade has been inserted along each drilling

2D inverse modeling

A tremendously important part of geo-electrical methods in recent years is increasingly the widespread application and inversion of Res and IP surveys (Loke & Barker, 2006), where simultaneous presentation of electrical resistivity and induced polarization properties can provide valuable insights about the geometry of sought targets in most metal-bearing deposits. Here, after electrical data acquisition, the data accuracy was checked, and then data processing was carried out. In first step, inversion was performed in 2D along all profiles to image electrical models across them at depth, where the least-squares method proposed by Loke, 2004 was run iteratively to converge a stabilized electrical model with a desired data misfit. After 5 iterations, the best sections selected such that recovered models could closely predict apparent electrical data. All profiles were stitched together and presented in Figs. 4a and 4b for electrical resistivity and chargeability, respectively. The results indicate that a positive relationship between the induced polarization and resistivity data exists for this case study, meaning that the sought Cu target may be a body in association with high value of the IP and Res models. For better checking the accuracy of 2D models, 3D visualization of predicted data along all profiles (Figs. 5a and 5c) versus the observed data (Figs. 5b and 5d) after running a 2D inversion algorithm were plotted, showing good matching between observed and predicted data for both electrical data.

3D geostatistical interpolation of 2D electrical data

In geostatistical interpolation, the desired variable must have spatial continuity to be appropriate for the use of geostatistical method, where a variogram model is assumed to seek its spatial structure. As it provides critical parameters for running various kriging estimators, the accuracy of the extracted parameters from the variogram is of crucial importance and can have significant impact on the estimated variable (Mostafaie et al., 2014). For this purpose, the data were reviewed. In the first stage, variography was done. Through trial-and-test examination of

electrical variables, experimental directional semi-variogram of the Res and IP generated from 2D inversion models, were plotted respectively in Figs. 6a and 6b. Note that at azimuth and dip of 0 and 20 degrees respectively, both electrical data had the highest spatial continuity, which indeed reflect the effect of N-S electrical profiles. A repetitive electrical resistivity patches (Fig. 4a) lead to a hole effect at the end of variography curve in Fig.6a, where variogram values fluctuate. Table 2 presents all parameters of fitted variogram models, assuming a spherical one. The SGeMS software (an open access Stanford Geostatistical Modeling Software) was used to fit the spherical variogram as the best theoretical model on the basis of the least square differences. Assuming these variogram models, electrical models were interpolated in 3D for electrical resistivity (Fig. 7a) and chargeability (Fig. 7c).

Table 2. Parameters obtained for the variogram model of the electrical resistivity, chargeability, and Cu grade

Major Axis	Azimuth	Dip	Range	Sill	Nugget	Model
Res	0	20	400	1	0.1	Spherical
IP	0	20	400	1	0.1	Spherical
Cu	120	30	318	1	0.1	Spherical

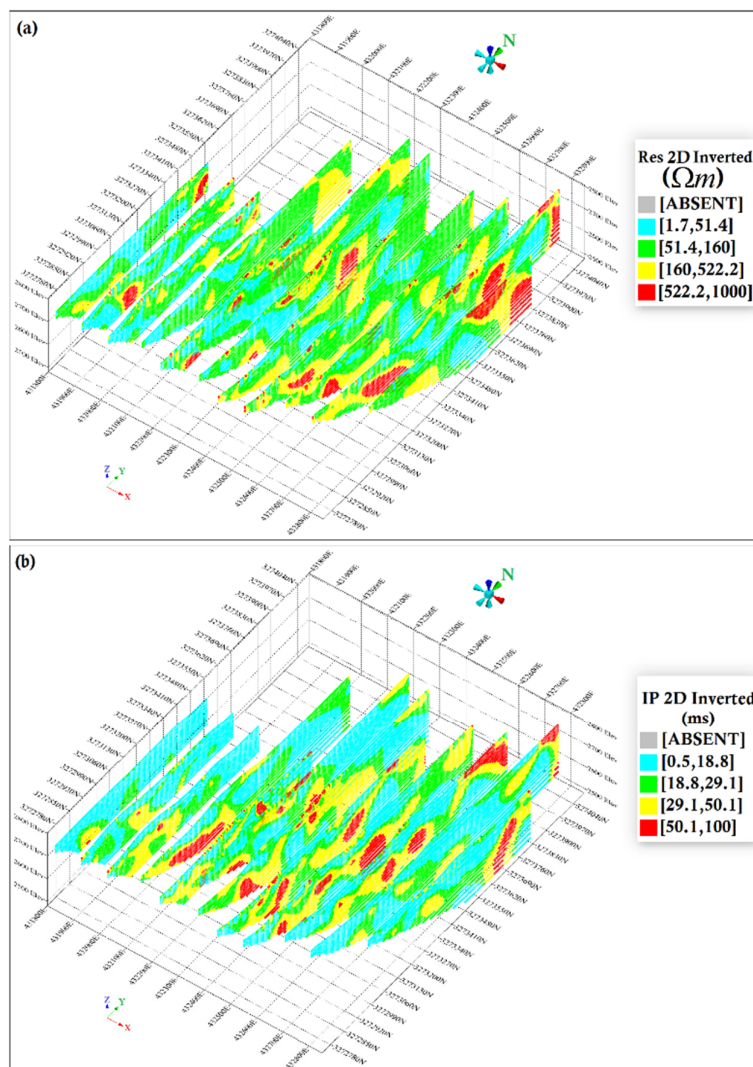


Figure 4. 3D visualization of all 2D inverted profiles of electrical resistivity (a), and chargeability (b)

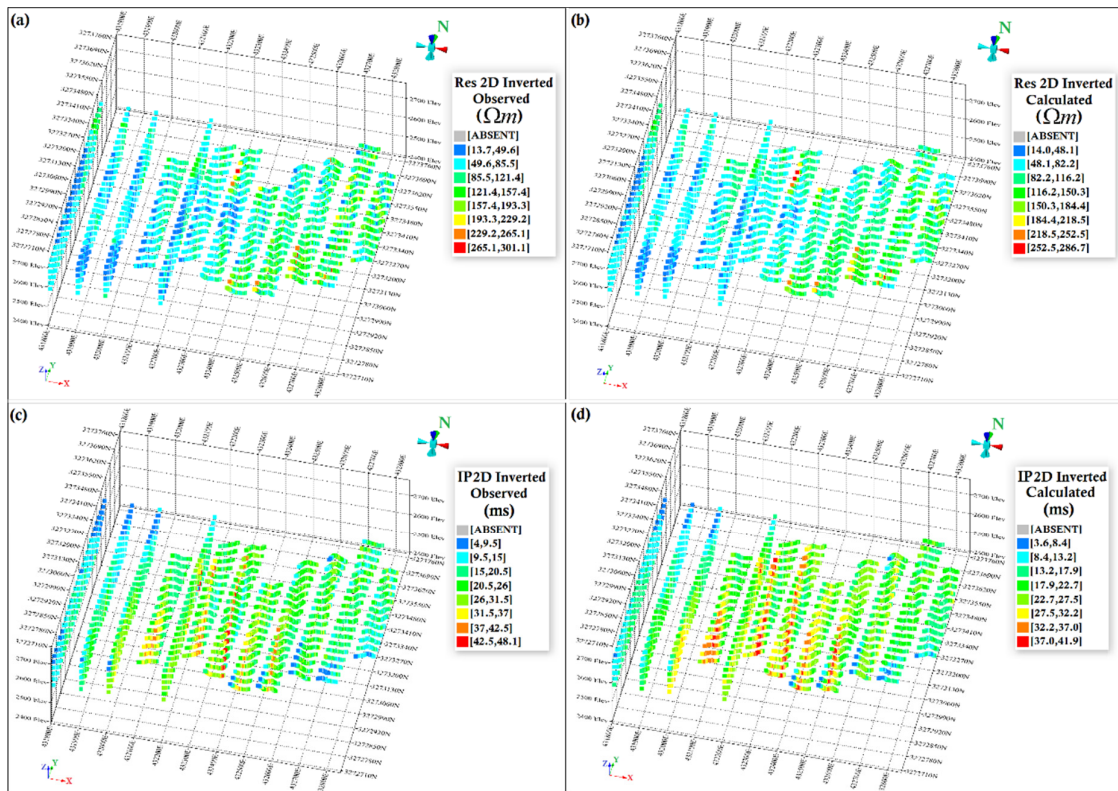


Figure 5. 3D visualization of predicted data versus the observed data for all 2D inverted profiles, where the left column presents the observed electrical resistivity (a), and chargeability (c), and the right one is for the predicted electrical resistivity (b), and chargeability (d)

Separation of the anomalous zone(s) (various populations in a domain) from the background setting are a key ingredient to exploration studies which determines the extent of sought mineralized targets. There are a set of statistically analytical methods such as probability plot, gap statistic, and analysis of variance for discretizing a desired model domain. These conventional methods have been highly applied in geochemical ones (where model domain is element concentration); however, they have been rarely used in geophysical analysis. The choice of method depends on the nature of data and purpose of the study. Due to the nature of data, different fractal methods have been popular for this purpose to discretize a desired domain into some populations (Daneshvar Saein & Afzal, 2017; Abdoli Sereshgi et al., 2019; Zadmehr & Shahrokhi, 2019; Saadati et al., 2020), where among them, the ‘‘Concentration–Number’’ (C–N) method (Hassanpour & Afzal, 2013) has been used in this research. The general form of the C–N fractal model can simply be described as follows:

$$N(\geq \beta) \propto \beta^{-\gamma} \quad (1)$$

where $N(\geq \beta)$ is the number of a quantity (such as Cu grade or geophysical models) greater than β value, which is a value of the desired element, and γ is a fractal dimension. The value must not endure any pretreatment, and results can be shown as a C–N log–log plot. This log–log plot represents element distribution and the relationship among different mineralized zones. These populations can be matched with geological characteristics of an ore occurrence system (Deng et al., 2010; Sadeghi et al., 2012; Hassanpour & Afzal, 2013; Afzal et al., 2016; Jebeli et al., 2018). The main advantage of this fractal model is the consideration of an overall structure of the data, without any preprocessing requirements (Mohammadpour et al., 2019).

The C–N fractal method was used to discretize the geophysical models into some populations. The logarithmic graphs are traced so that Res/IP values are on the horizontal axis and the

number is on the vertical axis. Breakpoint lines indicate changes in population; therefore, the breakpoint should be considered as the threshold, because the fractal dimension of anomaly is different from the fractal dimension of background. Fractal curves plotted in Figs. 7b and 7d have divided the geophysical models into four populations, while the reclassified physical models have the same spatial correlation. Note that higher values of the resistivity model (Fig. 7a) are matched with higher values of the chargeability (Fig. 7c) and vice versa.

On the basis of drilling results, an ordinary kriging was utilized to interpolate the Cu distribution in Fig. 8a, where the variography model plotted in Fig. 6c was assumed to estimate the Cu grade. Through a C-N analysis of the Cu grade (Fig. 8b), the Cu model has been divided into four zones whose populations are similar to the geophysical models.

According to the distance between the boreholes, the block models were constructed in length and width of 10 m, and height of 5 m to generate three aforementioned models (Figs. 7a, 7c, 8a). As mention, the fractal method was used in order to determine the threshold of data. Based on the plotted fractal curves, four zones were extracted from three models. Zone I, which includes values of 4.8–82.8 Ω .m (Res, Fig. 7a) and 0-19.9 ms (IP, Fig. 7b), shown in blue and bright blocks, was classified as the background.

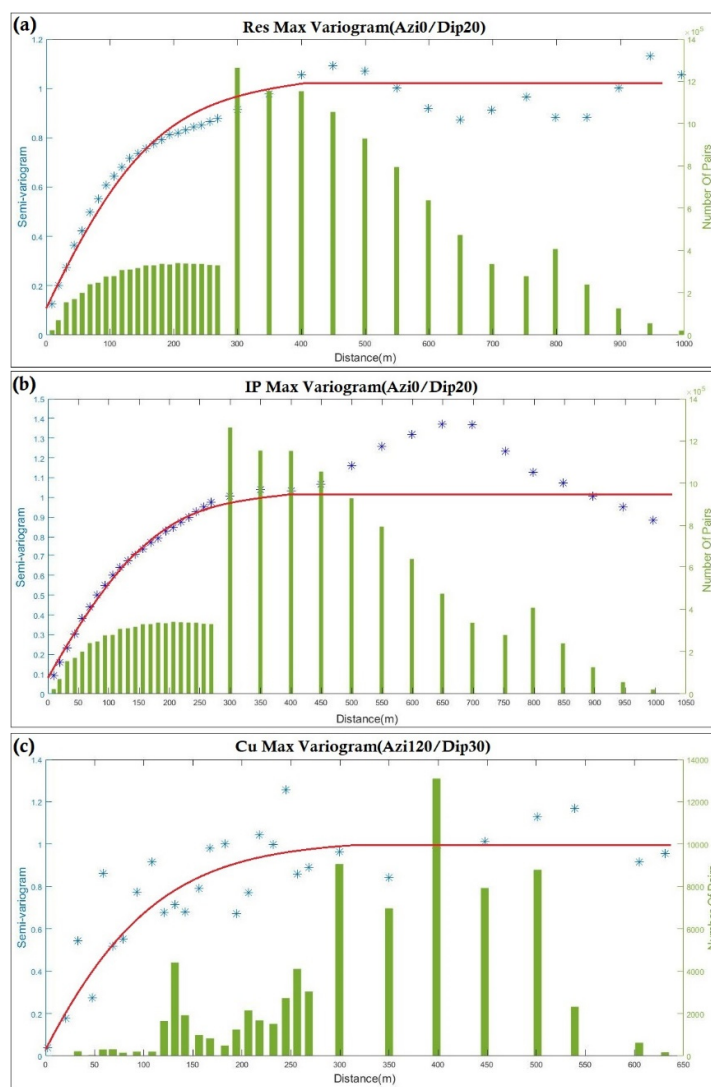


Figure 6. Experimental directional semi-variogram, models, and number of pairs along the main axis for the electrical resistivity (a), chargeability (b), and Cu grade (c)

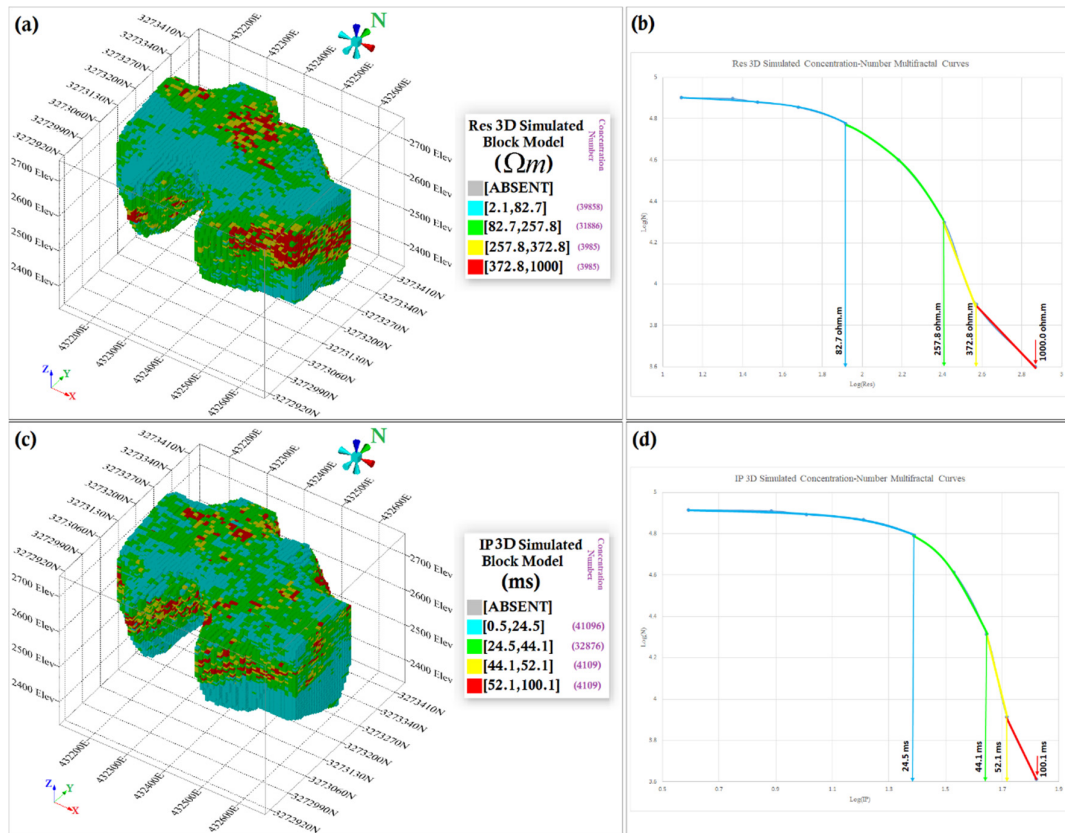


Figure 7. 3D modeling of geophysical properties of (a) electrical resistivity, and (c) chargeability through geostatistical interpolation of all 2D inverted data (left column), where their concentration-number multifractal curves (right column) were used to reclassify these properties (b) electrical resistivity, and (d) chargeability into its sub zones. The anomalous zone of each property has been shown in the left column

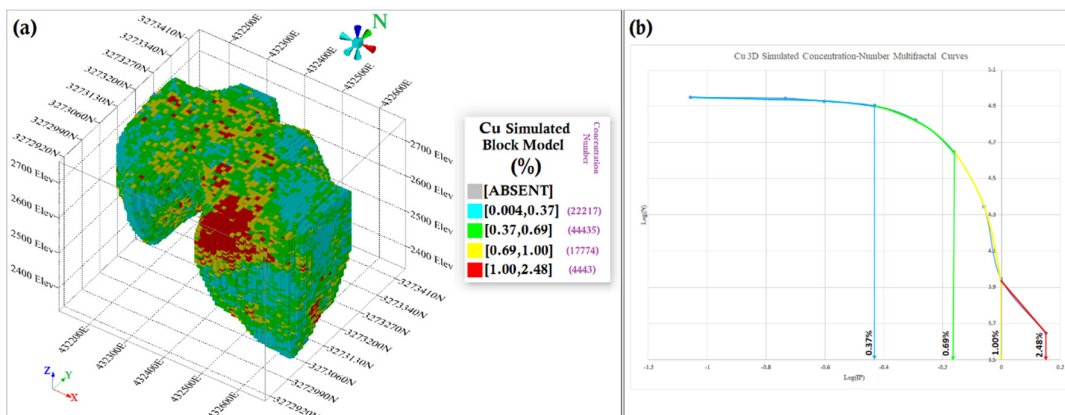


Figure 8. 3D visualization of the Cu concentration (a), reclassified by its concentration-number multifractal curve (b)

In zones II-III, the blocks are shown by the color green and yellow in the models. Threshold values of Res are 82.8 to 413.8 $\Omega.m$, and IP includes the values between 19.9 to 53.1 ms. Zone IV includes high intensity anomaly shown by red blocks in both models. High-intensity anomaly is determined by a value of over 413.8 $\Omega.m$ in the Res model and more than 53.1 ms in the IP model. According to the models, there is a mineralization body with an E-W strike. This body starts from a depth of 50 m, and the 3D model shows that it is a continuous

mineralization body. In the center to southeast part of the area, there is an anomalous region with a high value of IP and Res. Table 1 has tabulated the statistical summaries of the 3D interpolated models as well. Based on the Cu model shown in Fig.8, four zones were separated. Zone I, which includes values of 0–0.3%, is shown in blue and bright blocks classified as the background. For zones II-III, the Cu values are shown by the blocks of green and yellow colors, with breakpoints at values of 0.3 and 1.02%. Zone IV includes high intensity Cu grade shown by red blocks in the model with values more than 1.02 %.

For better interpretation of the geophysical models and Cu distribution, a cross section in the block model was chosen as a representative of all profiles, where some exploratory boreholes have located along the extracted electrical profile (Fig. 9). As can be seen, those regions with higher grade of Cu mineralization (Fig. 9e) are partially correlated with high values of the electrical resistivity (Fig.9a) and chargeability (Fig.9b), respectively. Such geophysical signatures are usually common in disseminated nature of Cu-bearing mineralization (Babaei et al., 2019).

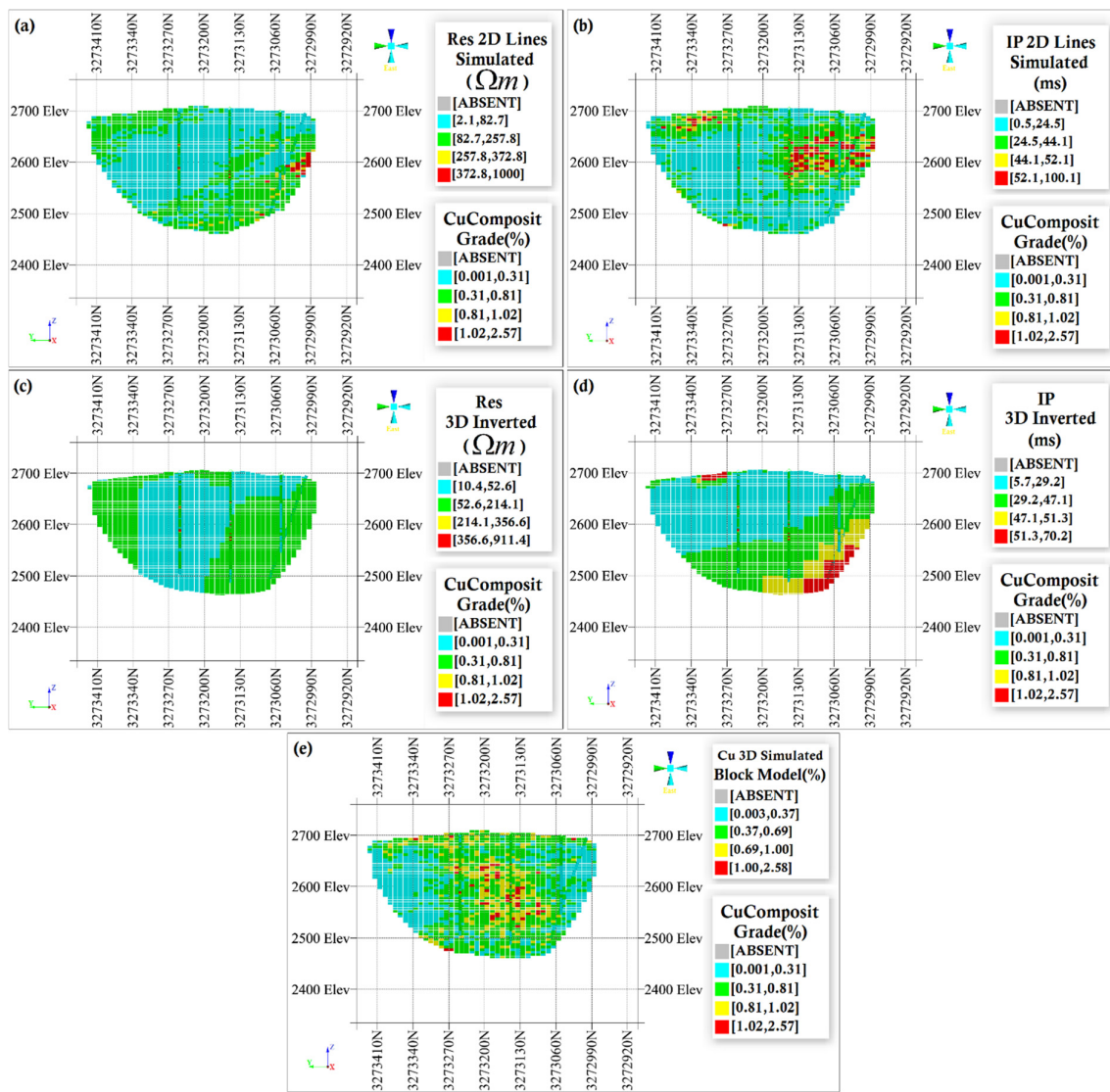


Figure 9. A cross-section view at the middle of the main source of Cu mineralization, (a) electrical resistivity from 3D interpolation, (b) chargeability form 3D interpolation, (c) electrical resistivity from 3D inversion, (d) chargeability from 3D inversion, and (e) interpolated Cu grade

3D inverse modeling

In this stage, electrical data were inverted in 3D through a smoothness constrained least-square optimization algorithm as it was expected to have a gradual resistivity variation in the subsurface (Loke et al., 2018). To run the inversion algorithm, an initial damping factor was set to 0.150, and a non-uniform grid was designed to discretize physical models into rectangle cube cells. In most electrical algorithms, the model parameters are the logarithms of the resistivity (Sasaki, 1994; Zhang et al., 1995; Loke & Barker, 1996; Pain et al., 2002; Gunther et al., 2006) since resistivity values vary over several orders of magnitude. Thus, the logarithms of apparent resistivity are used to prevent very large values from having an overwhelming influence on the inversion process, note that the use of logarithms has the additional advantage of introducing positivity constraints on the model parameters as well (Ramazi & Jalali, 2015).

To compare the electrical models from 3D inversion with the 3D interpolation, the 3D inversion of electrical data was performed. The inversion was completed after 6 iterations with the RMS errors of 10.1% and 3.46% for resistivity and chargeability models, respectively. Results of 3D inversion are shown in Figs.10a and 10b for electrical resistivity and chargeability, respectively. For better checking of the accuracy of 3D models, predicted data were plotted versus the observed ones in Fig. 11 along all electrical profiles, showing low misfit error of inverted models.

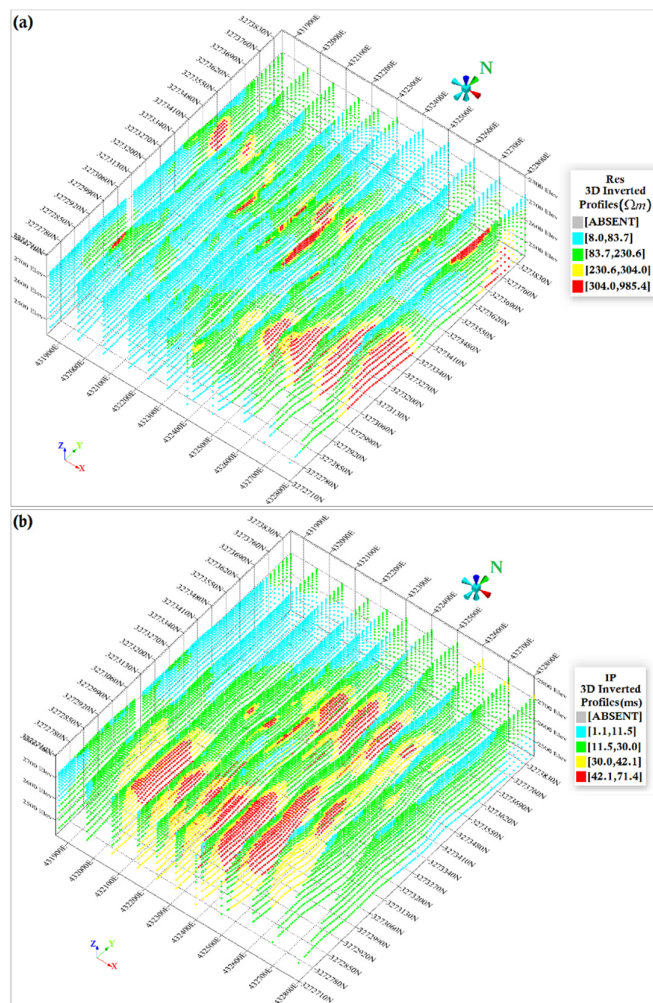


Figure 10. 3D visualization of all 3D inverted profiles of electrical resistivity (a), and chargeability (b), along surveyed profiles

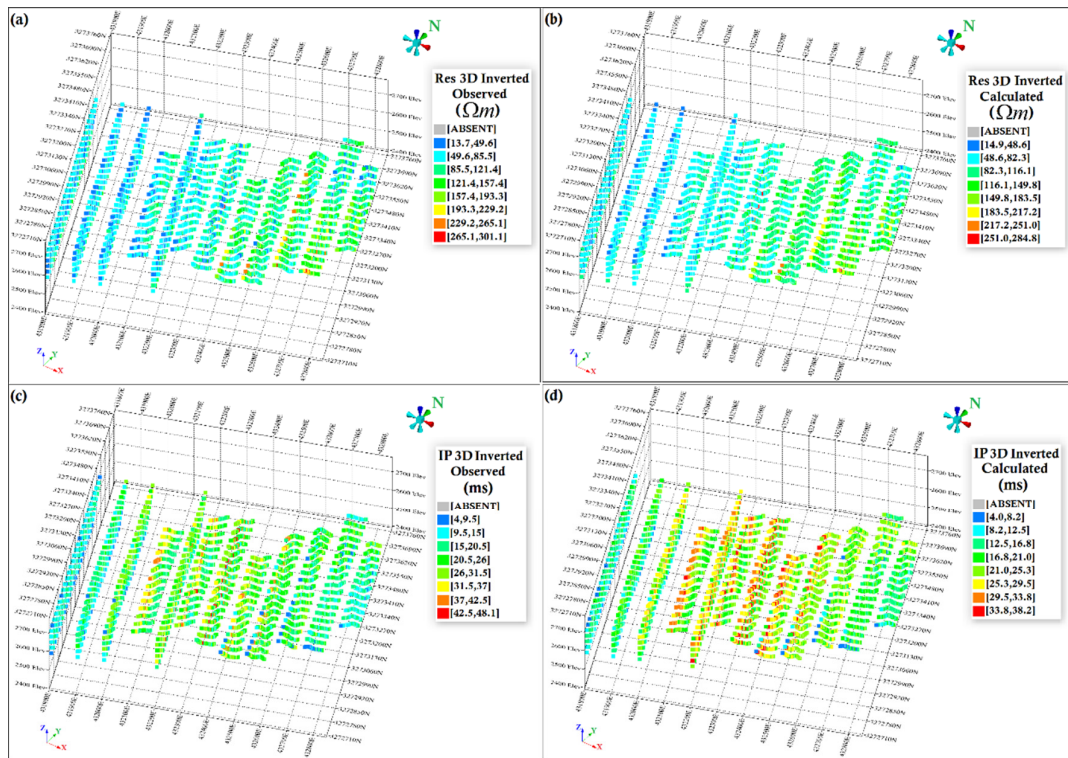


Figure 11. 3D visualization of predicted data versus the observed data for all 3D inverted profiles, where the left column presents the observed electrical resistivity (a), and chargeability (c), and the right one is for the predicted electrical resistivity (b), and chargeability (d)

The block model that has been constructed earlier was used to assign value of 3D inverted properties to all blocks, where the Res and IP models derived from 3D inversion have been shown in Figs. 12a and 12c, respectively. Table 1 has tabulated the statistical summaries of the 3D inverted models. Fractal curves of these models (Figs. 12b and 12d) have divided the physical models into four zones. It is worth noting that these physical models could much better present the continuity of desired zones compared to ones derived from the 3D interpolation (Figs. 7a and 7c). For better visualization of this superiority, the physical models from 3D inversion were extracted along previous cross-section (Figs. 9c and 9d), showing more spatial correlation of anomalous zones of electrical models with the Cu grade (Fig. 9e).

Discussion

The Takht-e-Gonbad porphyry-type Cu deposit in Iran was investigated in this study to construct its geometry through geophysical models of electrical resistivity and chargeability, whose Cu-bearing mineralization zones have meaningful geo-electrical footprints. In the first stage, the IP and Res sections were prepared by a 2D inverse modeling approach, while 2D sections showed that high IP and Res values are consistent with higher grade of Cu mineralization. 3D models of Res and IP data then were interpolated in 3D through an ordinary kriging geostatistical method. The 3D block models of Res and IP were constructed from interpolated models to compare them with blocky model of Cu grade, showing that the geostatistical estimation is smoothing and partially correlated with the distribution of Cu enrichment in the studied area.

In the next stage to characterize better the mineralization zones, especially mineralization situation at the distance between profiles, the 3D inversion routine was implemented for electrical data.

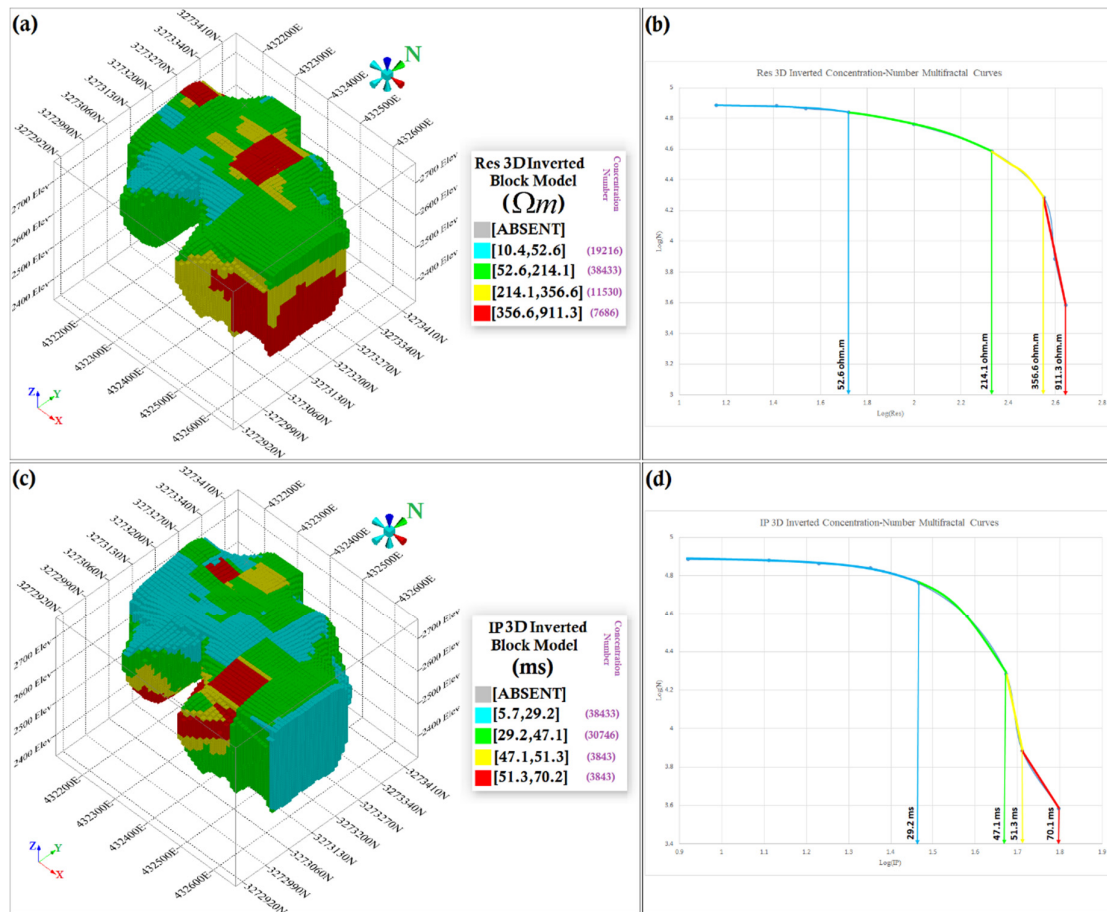


Figure 12. 3D modeling of geophysical properties of (a) electrical resistivity, and (c) chargeability through 3D inversion (left column), where their concentration-number multifractal curves (right column) were used to reclassify these properties (b) electrical resistivity, and (d) chargeability into its sub zones. The anomalous zone of each property has been shown in the left column

The 3D inverted models confirmed the 2D inverted models to some extent. As shown in Fig. 13, the scatter plots of electrical models derived from 3D inversion versus the ones acquired from 3D interpolation have partial correlation, indicating that interpolated data can substantially differ from the inverted models. Superiority of 3D inversion over the geostatistical interpolation is evident in scatter plots shown in Fig. 14, where the pairwise correlation of 3D inverted models versus the Cu grade are depicted for inversion and interpolation cases. Note that a positive coefficient exists in all plots, meanwhile this coefficient is higher for models derived from 3D inversion. Thus, it can be inferred that 3D inversion can much better preserve the geometry of sought Cu-bearing zones which have significant electrical signatures. The anomalous zones of Cu mineralization are traced with zones of high values of both the Res and IP properties.

Another point should be noted is that the 3D inversion lacks the ideal specifications required for a reliable 3D inverse modeling. The electrode spacing in 3D inverse modeling was 10 m, but the profile spacing was 30 m. That is not consistent with the proposed limits by Bentley & Gharibi, 2004 and Gharibi & Bentley, 2005, where the spacing between parallel profiles should not exceed more than twice of the unit electrode spacing. Despite the spacing was a bit more than the recommended distance, electrical models both in 2D and 3D could provide reliable outcomes for imaging of anomalous geophysical zones which were spatially in association with Cu occurrences.

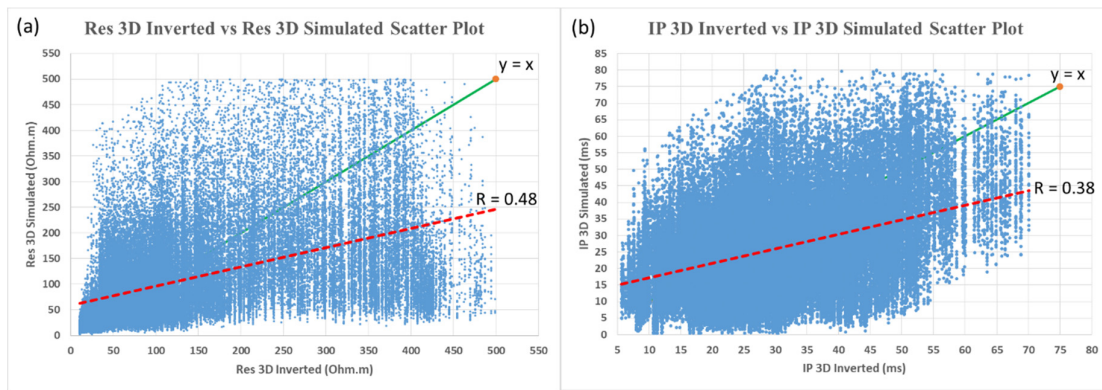


Figure 13. The scatter plot of the electrical properties from 3D inversion versus 3D interpolation through geostatistics, (a) electrical resistivity, and (b) chargeability

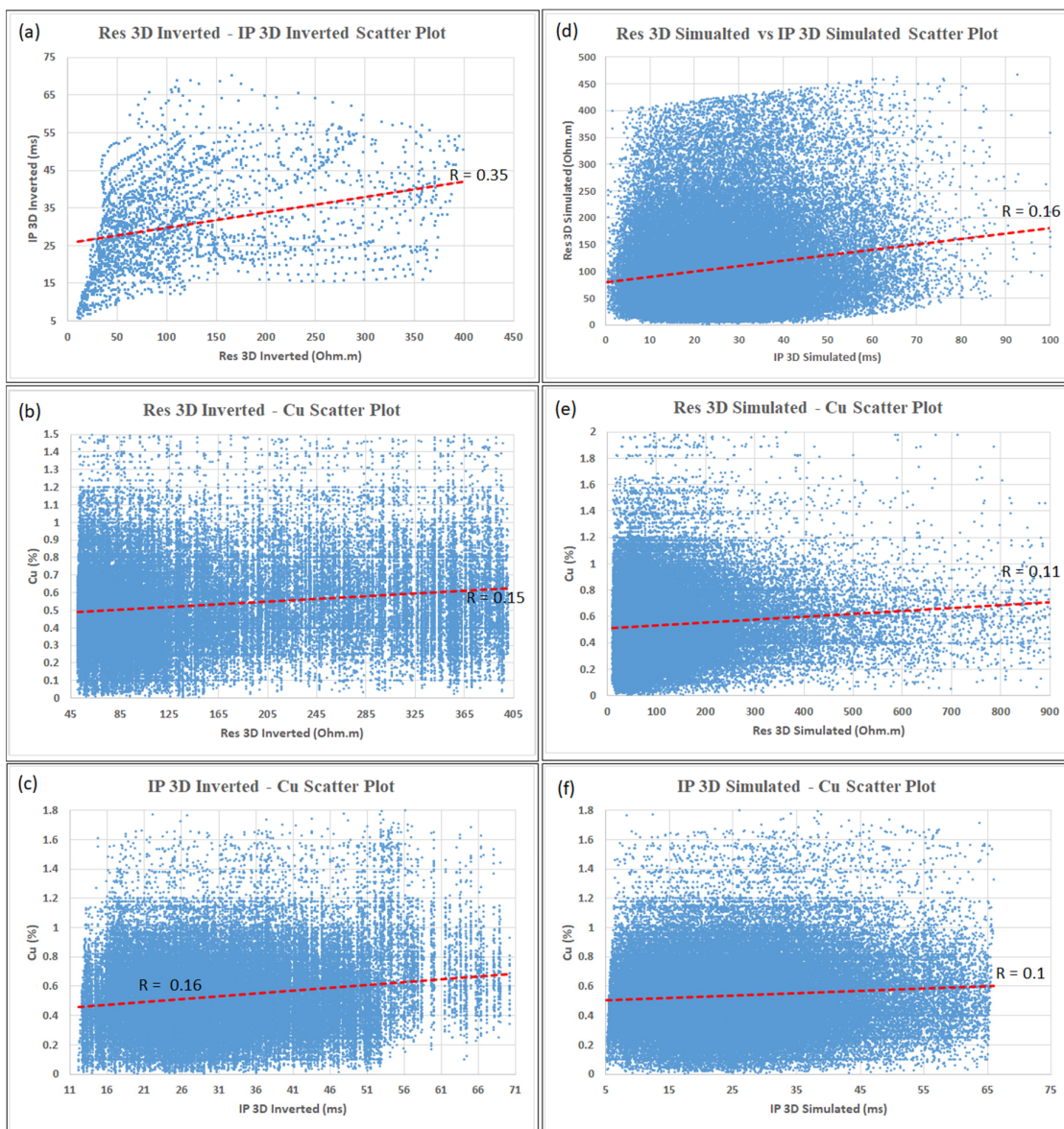


Figure 14. Scatter plots between (a) RS-IP, (b) RS-Cu, and (c) IP-Cu, from 3D inversion of the electrical data (left column) and the similar plots from 3D interpolation (d) RS-IP, (e) RS-Cu, and (f) IP-Cu, in right column. Pearson's correlation coefficient between each model has been calculated

Conclusion

The mineralization zones in the Takht-e-Gonbad copper deposit is successfully localized by integrating time-domain induced polarization and electrical resistivity models. A fractal model (i.e. concentration-number) method was used for dividing geophysical and Cu grade models into four populations where anomalous Cu-bearing zones were matched with more resistive and chargeable zones. Electrical models were constructed in two ways from 3D inversion and 3D geostatistically interpolation indicating that 3D inversion could better present and preserve the geometry of Cu-bearing zone in the Takht-e-Gonbad porphyry deposit. The strike of Cu-bearing mineralization was in E-W direction with a disseminated nature of occurrences.

Acknowledgements

Authors would like to express their sincere thanks to the School of Mining Engineering, University of Tehran, for all supports.

References

- Abedi, M., Asghari, O., Norouzi, G.-H., 2015. Collocated cokriging of iron deposit based on a model of magnetic susceptibility: a case study in Morvarid mine, Iran. *Arabian Journal of Geosciences*, 8(4): 2179-2189.
- Afzal, P., Tehrani, M.E., Ghaderi, M., Hosseini, M.R., 2016. Delineation of supergene enrichment, hypogene and oxidation zones utilizing staged factor analysis and fractal modeling in Takht-e-Gonbad porphyry deposit, SE Iran. *Journal of Geochemical Exploration*, 161: 119-127.
- Aguilef, S., Vargas, J.A., Yáñez, G., 2017. Relationship between bulk mineralogy and induced polarisation responses in iron oxide-copper-gold and porphyry copper mineralisation, northern Chile. *Exploration Geophysics*, 48(4): 353-362.
- Alirezaei, S., Hassanpour, S., 2011. An overview of porphyry copper deposits in Iran. The 1st world copper congress, Iran.
- Asghari, O., Sheikhmohammadi, S., Abedi, M., Norouzi, G., 2016. Multivariate geostatistics based on a model of geo-electrical properties for copper grade estimation: a case study in Seridune, Iran. *Bollettino di Geofisica Teorica ed Applicata*, 57(1): 43-58.
- Babaei, M., Abedi, M., Norouzi, G.-H., Kazem Alilou, S., 2019. Geostatistical modeling of electrical resistivity tomography for imaging porphyry Cu mineralization in Takht-e-Gonbad deposit, Iran. *Journal of Mining and Environment*, 11: 143-159.
- Bentley, L.R., Gharibi, M., 2004. Two-and three-dimensional electrical resistivity imaging at a heterogeneous remediation site. *Geophysics*, 69(3): 674-680.
- Daneshvar Saein, L., Afzal, P., 2017. Correlation between Mo mineralization and faults using geostatistical and fractal modeling in porphyry deposits of Kerman Magmatic Belt, SE Iran. *Journal of Geochemical Exploration*, 181: 33-343.
- deGroot-Hedlin, C., Constable, S., 1990. Occam's inversion to generate smooth, two-dimensional models from magnetotelluric data. *Geophysics*, 55(12): 1613-1624.
- Deng, J., Wang, Q., Yang, L., Wang, Y., Gong, Q., Liu, H., 2010. Delineation and explanation of geochemical anomalies using fractal models in the Heqing area, Yunnan Province, China. *Journal of Geochemical Exploration*, 105(3): 95-105.
- Fakhari, S., Jafarirad, A., Afzal, P., Lotfi, M., 2019. Delineation of hydrothermal alteration zones for porphyry systems utilizing ASTER data in Jebal-Barez area, SE Iran. *Iranian Journal of Earth Sciences*, 11: 80-92.
- Gharibi, M., Bentley, L.R., 2005. Resolution of 3-D electrical resistivity images from inversions of 2-D orthogonal lines. *Journal of Environmental and Engineering Geophysics*, 10(4): 339-349.
- Gunther, T., Rucker, C., Spitzer, K., 2006. Three-dimensional modelling and inversion of dc resistivity data incorporating topography—II. Inversion. *Geophysical Journal International*, 166(2): 506-517.
- Hassanpour, S., Afzal, P., 2013. Application of concentration–number (C–N) multifractal modeling for

- geochemical anomaly separation in Haftcheshmeh porphyry system, NW Iran. *Arabian Journal of Geosciences*, 6(3): 957-970.
- Hosseini, M., 2012. Mineralogy, geochemistry, fluid inclusion and genesis of Takht-e-Gonbad copper deposit, northeast Sirjan (M. Sc. thesis). Tarbiat Modares University, Tehran, Iran, 257 p.
- Hosseini, M., Ghaderi, M., Alirezaei, S., 2011. Geology, alteration and mineralization characteristics of Takht-e-Gonbad copper deposit, northeast Sirjan. *Proceedings of the 1st World Copper Congress*, Tehran, Iran.
- Hosseini, M.R., Ghaderi, M., Alirezaei, S., Sun, W., 2017. Geological characteristics and geochronology of the Takht-e-Gonbad copper deposit, SE Iran: A variant of porphyry type deposits. *Ore Geology Reviews*, 86: 440-458.
- Izadi Yazdanabadi, M., Hojat, A., Ranjbar, H., Karimi Nasab, S., 2017. A Geographic Information System-based site selection experience for the construction of a geomagnetic observatory in Kerman Province, Iran. *Geophysical Prospecting*, 65: 237-245.
- Jebeli, M., Afzal, P., Pourkermani, M., Jafari Rad, A., 2018. Correlation between rock types and Copper mineralization using fractal modeling in Kushk-e-Bahram deposit, Central Iran. *Geopersia*, 8(1): 131-141.
- Loke, M., Barker, R., 2006. Rapid least-squares inversion of apparent resistivity pseudosections by a quasi-Newton method. *Geophysical Prospecting*, 44(1): 131-152.
- Loke, M., Wilkinson, P., Chambers, J., Meldrum, P., 2018. Rapid inversion of data from 2D resistivity surveys with electrode displacements. *Geophysical Prospecting*, 66(3): 579-594.
- Loke, M.H., 2004. Tutorial: 2-D and 3-D electrical imaging surveys.
- Loke, M.H., Acworth, I., Dahlin, T., 2003. A comparison of smooth and blocky inversion methods in 2D electrical imaging surveys. *Exploration geophysics*, 34(3): 182-187.
- Loke, M.H., Barker, R.D., 1996. Rapid least-squares inversion of apparent resistivity pseudosections by a quasi-Newton method. *Geophysical prospecting*, 44(1): 131-152.
- Mohammadi, N.M., Hezarkhani, A., 2018. Application of support vector machine for the separation of mineralised zones in the Takht-e-Gonbad porphyry deposit, SE Iran. *Journal of African Earth Sciences*, 143: 301-308.
- Mohammadpour, M., Bahroudi, A., Abedi, M., Rahimpour, G., Jozanikohan, G., Khalifani, F.M., 2019. Geochemical distribution mapping by combining number-size multifractal model and multiple indicator kriging. *Journal of Geochemical Exploration*, 200: 13-26.
- Mostafaie, K., Ramazi, H., 2015. Application of electrical resistivity method in sodium sulfate deposits exploration, case study: Garmab, Iran. *Journal of Biodiversity and Environmental Sciences*, 6(2): 2220-6663.
- Mostafaie, K., Ramazi, H. R., Jalali, M., 2014. Application of integrated geophysical and geostatistical methods in Amiriyeh site classification. *Geodyn Res Int Bull (GRIB)*, 2(2): 1-15.
- Oldenburg, D.W., Li, Y., Ellis, R.G., 1997. Inversion of geophysical data over a copper gold porphyry deposit: a case history for Mt. Milligan. *Geophysics*, 62(5): 1419-1431.
- Pain, C.C., Herwanger, J.V., Worthington, M.H., Oliveira, C.R.d., 2002. Effective multidimensional resistivity inversion using finite-element techniques. *Geophysical Journal International*, 151(3): 710-728.
- Ramazi, H., Jalali, M., 2015. Contribution of geophysical inversion theory and geostatistical simulation to determine geoelectrical anomalies. *Studia Geophysica et Geodaetica*, 59(1): 97-112.
- Ranjbar, H., Honarmand, M., Moezifar, Z., 2004. Application of the Crosta technique for porphyry copper alteration mapping, using ETM+ data in the southern part of the Iranian volcanic sedimentary belt. *Journal of Asian Earth Sciences*, 24(2): 237-243.
- Saadati, H., Afzal, P., Torshian, H., Solgi, A., 2020. Geochemical exploration for Li using Geochemical Mapping Prospectivity Index (GMPI), fractal and Stage Factor Analysis (SFA) in NE Iran. *Geochemistry: Exploration, Environment, Analysis*, 20: 461-472.
- Sadeghi, B., Moarefvand, P., Afzal, P., Yasrebi, A.B., Saein, L.D., 2012. Application of fractal models to outline mineralized zones in the Zaghia iron ore deposit, Central Iran. *Journal of Geochemical Exploration*, 122: 9-19.
- Saein, L.D., Rasa, I., Omran, N.R., Moarefvand, P., Afzal, P., 2012. Application of concentration-volume fractal method in induced polarization and resistivity data interpretation for Cu-Mo porphyry deposits exploration, case study: Nowchun Cu-Mo deposit, SE Iran. *Nonlinear Processes in*

- Geophysics, 19(4): 431-438.
- Saric, V., Mijalkovic, N., 1973. Metallogenic map of Kerman region, 1: 500000 scale. Exploration for ore deposits in Kerman region. Geol Surv Iran Rep, 53: 247.
- Sasaki, Y., 1992. RESOLUTION OF RESISTIVITY TOMOGRAPHY INFERRED FROM NUMERICAL SIMULATION 1. Geophysical prospecting, 40(4): 453-463.
- Sasaki, Y., 1994. 3-D resistivity inversion using the finite-element method. Geophysics, 59(12): 1839-1848.
- Sereshgi, H.A., Ganji, A., Ardalan, A.A., Torshizian, H., Taheri, J., 2019. Detection of metallic prospects using staged factor and fractal analysis in Zouzan region, NE Iran. Iranian Journal of Earth Sciences, 11: 256-266.
- Sultan, S.A., Mansour, S.A., Santos, F.M., Helaly, A.S., 2009. Geophysical exploration for gold and associated minerals, case study: Wadi El Beida area, South Eastern Desert, Egypt. Journal of Geophysics and Engineering, 6(4): 345-356.
- Telford, W.M., Telford, W., Geldart, L., Sheriff, R.E., Sheriff, R., 1990. Applied geophysics, Cambridge university press.
- Zadmehr, F., Shahrokhi, S.V., 2019. Separation of geochemical anomalies by concentration-area and concentration-number methods in the Saqez 1:100,000 sheet, Kurdistan. Iranian Journal of Earth Sciences 11: 196-204.
- Zhang, J., Mackie, R. L., Madden, T.R., 1995. 3-D resistivity forward modeling and inversion using conjugate gradients. Geophysics, 60(5): 1313-1325.



This article is an open-access article distributed under the terms and conditions of the Creative Commons Attribution (CC-BY) license.